RSC Advances

PAPER

View Article Online
View Journal | View Issue

Cite this: *RSC Adv.*, 2025, **15**, 9891

Anchored epitaxial growth of single-oriented one-dimensional organic nanowires towards their integration into field-effect transistors and polarization-sensitive photodetector arrays†

Phetluengxay Keo,‡[a] Tingyi Yan,‡[a] Jinwen Wang,*[a] Xiujuan Zhang,[a] Yandi Shi*[a] and Jiansheng Jie*[ab]

The deliberate assembly of organic small molecules into single-oriented one-dimensional (1D) nanowires is essential for the large-scale, on-chip integration of organic nanowire-based (opto)electronic devices. However, achieving single-oriented 1D organic nanowires remains a considerable challenge, predominantly attributed to the intricate nucleation and growth behaviors of the molecules. Herein, an anchored epitaxial growth method was developed to facilitate the single-oriented growth of 1D organic nanowires using the parallel nanogrooves on the annealed sapphire as anchoring seed crystal templates. The depth of the nanogrooves was greater than the length of the molecules, enabling the molecules to be embedded into the V-shaped nanogrooves and to form anchored nuclei during the physical vapor deposition process. Subsequently, these nuclei exhibited directional epitaxial growth along the nanogrooves, resulting in the formation of single-oriented 1D organic nanowires. Various organic small molecule 1D nanowires with uniform molecular packing and orientation were obtained and utilized for subsequent device integration. 2,7-Dioctyl[1]benzothiophene (C8-BTBT) was used as a model material, and the flexible organic field-effect transistor (OFET) based on the single C8-BTBT nanowire exhibited a mobility of up to 1.5 $cm^2 V^{-1} s^{-1}$. Benefiting from high mobility and uniform orientation, the integrated polarization-sensitive photodetector arrays based on 1D C8-BTBT nanowires exhibited a high dichroic ratio of up to 2.83, which was higher than those of some previously investigated 1D nanowires and two-dimensional materials. This work presents new opportunities to fabricate single-oriented 1D organic nanowires for integrated devices.

Received 26th November 2024
Accepted 17th March 2025

DOI: 10.1039/d4ra08354g

rsc.li/rsc-advances

Introduction

One-dimensional (1D) organic nanowires, boasting intrinsic flexibility, long-range ordered structure, absence of grain boundaries, and low defect density, hold great promise as fundamental building blocks for the development of functional (opto)electronic devices.[1–4] In particular, owing to their anisotropic geometry, small dimensions and high crystallinity, devices based on 1D organic nanowires exhibit superior performance compared with their bulk counterparts.[5–7] Unlike conventional inorganic nanowires (*e.g.*, silicon nanowires), 1D organic nanowires can be directionally grown at lower temperatures without metal catalysts.[8–10] This allows *in situ* growth on the temperature-sensitive flexible substrates.[11,12] In addition, integrating the single-oriented organic single nanowires into the functional electronic devices presents new opportunities for the development of high-performance field-effect transistors,[13] polarized photodetectors,[14] and the emerging stretchable artificial synapses[15] while enabling device miniaturization for lightweight and compact designs.[16,17]

Up to now, extensive research has been conducted on a range of 1D organic nanowires, with a particular focus on crystal synthesis and structure construction.[18,19] However, the complex nucleation and growth behaviors observed in these nanowires often result in the random alignment of the nanowires, which in turn limits the potential for the efficient carrier transport within the material.[20,21]

In recent decades, significant research has been conducted with the objective of aligning and integrating 1D organic nanowires into practical planar devices. The relevant methods can be classified into two principal branches, namely, solution-processing techniques and physical vapor deposition (PVD) strategies. Solution-processing techniques make full use of laminar flow,

[a]*Institute of Functional Nano & Soft Materials (FUNSOM), Jiangsu Key Laboratory for Carbon-Based Functional Materials & Devices, Soochow University, Suzhou, Jiangsu 215123, P. R. China. E-mail: jsjie@suda.edu.cn*

[b]*Macao Institute of Materials Science and Engineering (MIMSE), MUST-SUDA Joint Research Center for Advanced Functional Materials, Macau University of Science and Technology, Taipa, Macau SAR 999078, P. R. China*

† Electronic supplementary information (ESI) available. See DOI: https://doi.org/10.1039/d4ra08354g

‡ The authors contributed equally to this work.

capillary force or solvent wetting/dewetting patterns on a substrate to drive the ordered self-assembly of organic molecules.[22–24] Despite the success of solution-processing techniques in producing aligned nanowires on a variety of substrates,[25–28] the single-oriented alignment remains susceptible to disruption by the turbulent mass transport in organic solution[29] or structural defects on the substrate[30] due to the relatively weak molecular interactions. Beyond that, the solvent molecules would inevitably be introduced into the organic nanowires, exhibiting a detrimental effect on carrier transport.[31] To achieve the single-oriented growth of high-quality nanowires, PVD methods have been developed using seed crystals to guide the epitaxial growth of 1D organic nanowires.[2,32] Nevertheless, the ability to align as-prepared 1D organic nanowires needs to be further enhanced due to the weak confined growth behavior on the target substrate.[32,33] Given the remarkable anisotropy of the charge transport behavior observed in organic crystalline semiconductors,[34] it is evident that the mobilities could vary by a factor of several orders of magnitude along different crystal orientations.[35] Therefore, the preparation of single-oriented 1D organic nanowires is very important to facilitate an improvement in device performance.

In this work, the anchored epitaxial growth strategy was developed to facilitate the single-oriented growth of 1D organic nanowires using the parallel nanogrooves on the annealed sapphire as the anchored seed crystal templates. The depth of the nanogrooves exceeded the length of the molecules, enabling the molecules embedded into the V-shaped nanogrooves to form anchored nuclei during the physical vapor deposition process. Subsequently, these nuclei exhibited directional epitaxial growth along the nanogrooves, resulting in the formation of single-oriented 1D organic nanowires. Various organic small molecule 1D nanowires with uniform molecular

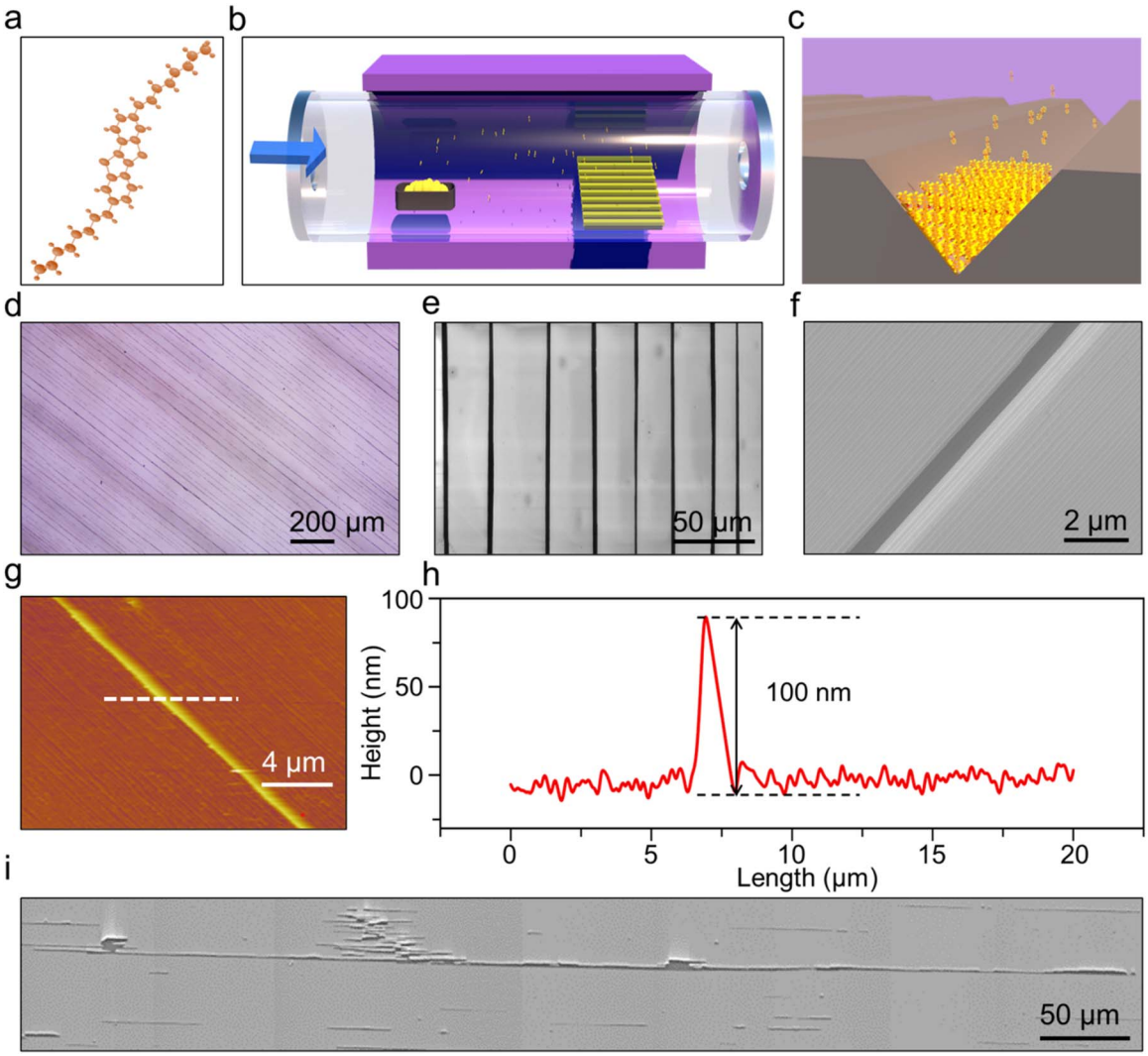

Fig. 1 (a) Structure of the C8-BTBT molecule. (b) Schematic of the single-oriented growth of C8-BTBT nanowire arrays *via* the physical vapor deposition method. (c) Schematic of the periodic V-shaped nanogrooves confining the 1D growth of the C8-BTBT molecules. (d) OM image of the as-grown C8-BTBT nanowire arrays with a consistent orientation on the *m*-plane sapphire substrate. (e) SEM image of the C8-BTBT nanowire arrays. (f) High-magnification SEM image of one of the typical C8-BTBT nanowires. (g) AFM image of one of the typical C8-BTBT nanowires on the *m*-plane sapphire substrate. (h) Height profile of the C8-BTBT nanowires on the *m*-plane sapphire substrate. (i) Stitched SEM images of one of the typical C8-BTBT nanowires on the *m*-plane sapphire substrate.

packing and orientation, namely, 2,7-(1-octyl)[1]benzothieno[3,2-*b*][1]benzothiophene (C8-BTBT), 2,6-diphenylanthracene (DPA), 2,9-didecyldinaphtho[2,3-*b*:2′,3′-*f*]thieno[3,2-*b*]thiophene (diF-TES-ADT), and 2,8-difluoro-5,11-bis(triethylsilylethynyl) anthradithiophene (C10-DNTT) nanowires, were notably obtained and were beneficial for subsequent diverse device integration. Using C8-BTBT as a model material, the flexible organic field-effect transistor based on the C8-BTBT nanowires exhibited a mobility up to 1.5 $cm^2\ V^{-1}\ s^{-1}$. Benefiting from high mobility and uniform orientation, the integrated polarization-sensitive photodetector arrays based on 1D C8-BTBT nanowires exhibited a high dichroic ratio of up to 2.83, which was higher than those of some investigated 1D nanowires and two-dimensional materials. This work paves the way for the monolithic fabrication of nanowire-based devices through the development of a novel approach for fabricating single-oriented 1D organic nanowires.

Results and discussion

The key to the successful preparation of single-oriented organic single-crystalline nanowires is the formation of appropriate nanostructures on the target substrate surface prior to the nanowire growth. To this end, the flat *M*-plane sapphires were initially subjected to an annealing process at 1400 °C for a period of 16 hours in ambient air. Due to the thermal instability of the $(10\bar{1}0)$ planes among the crystal facets of sapphire,[36] the spontaneous reconstruction of the surface atoms occurred,

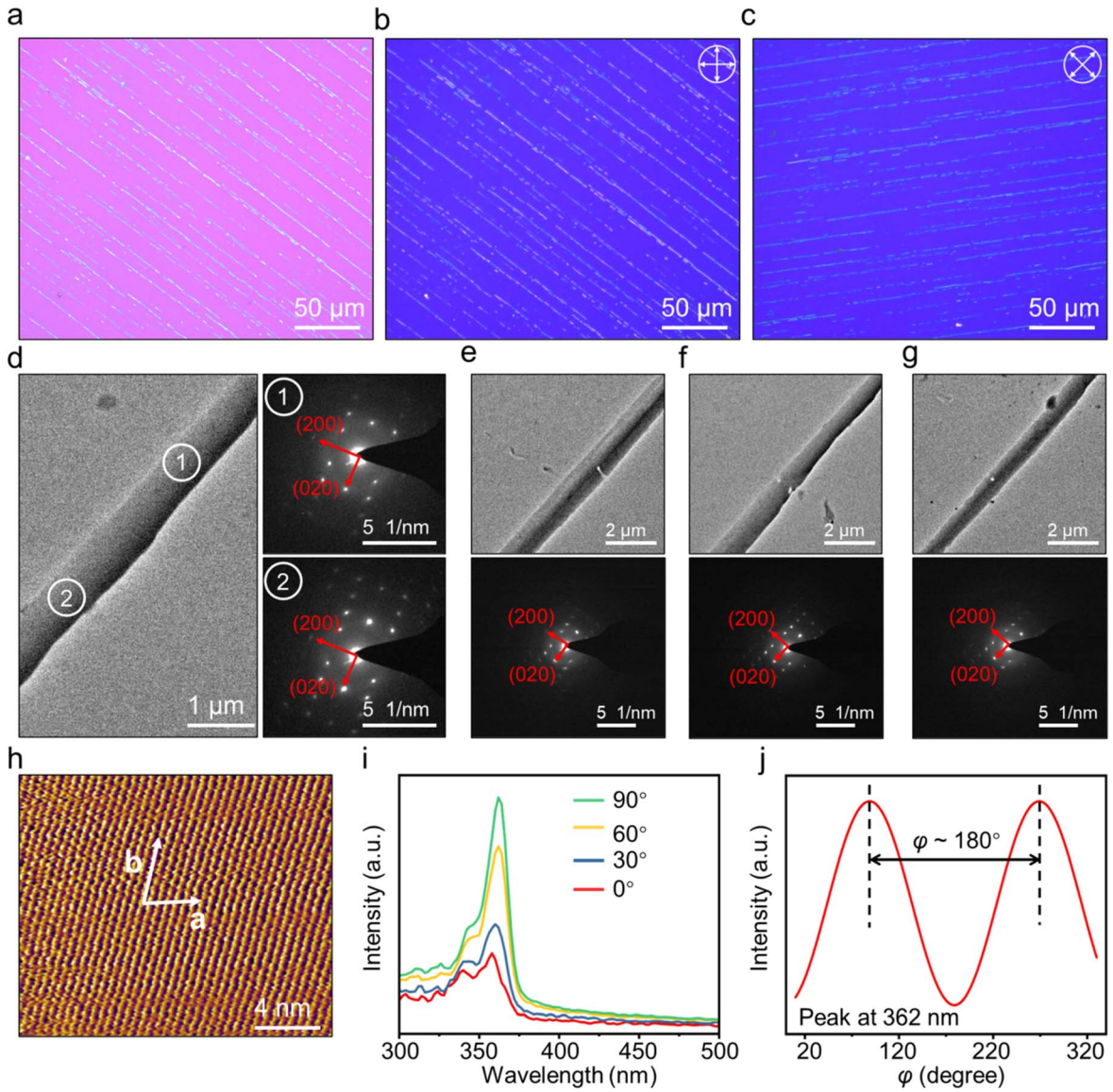

Fig. 2 (a) OM image of 1D C8-BTBT nanowires transferred to a SiO_2/Si substrate. (b and c) Angle-dependent polarized intensity of the 1D C8-BTBT nanowire. (d) TEM image of an individual C8-BTBT nanowire and its corresponding SAED patterns recorded from two different positions marked in (d). (e–g) TEM images (top) and SAED patterns (bottom) collected from the different C8-BTBT nanowires. (h) HR-AFM image of 1D C8-BTBT nanowires. (i) Polarized UV-vis absorption spectra of the 1D C8-BTBT nanowires. (j) Angle-resolved absorbance of the 1D C8-BTBT nanowires at an incident light wavelength of 362 nm.

resulting in the formation of the V-shaped nanogrooves on the sapphire surface (Fig. S1a†). Observation shows that the direction of these nanogrooves was in accordance with the [10$\bar{1}$0] orientation of the *m*-plane sapphire, thereby resulting in a substrate with an anisotropic character. The periodic nanogrooves exhibited a thickness of approximately 20 nm (Fig. S1b and c†).

As illustrated in Fig. 1a, the C8-BTBT molecule is composed of rigid π-conjugated skeletons and soft alkyl chains. This structural configuration enables the anisotropic interactions that exist within the crystals, namely, the out-of-plane weak van der Waals interactions between the alkyl chains and the in-plane strong intermolecular interactions between π-conjugated skeletons. In accordance with the principles of crystal growth kinetics, the rate of growth is greater on higher-energy faces. Consequently, the C8-BTBT molecules exhibited a proclivity for two-dimensional stacking and underwent spontaneous growth into lamellar crystals. To fabricate 1D organic nanowires with the single crystallographic orientation, the annealed sapphire, featuring the periodic V-shaped nanogrooves, was used as the growth template to confine the 1D growth of the molecules (Fig. 1b and c). Herein, high-purity C8-BTBT powder was used as a precursor, and a mixture of Ar and H_2 was used as the carrier gas. The C8-BTBT powder was heated to 120 °C in order to realize the phase transition into the smectic liquid crystal.[14] More details regarding the preparation of the nanowires can be found in the Experimental section (ESI).† Fig. 1d and e show the optical microscopy (OM) and scanning electron microscopy (SEM) images of 1D C8-BTBT nanowires grown on the *m*-plane sapphire substrate, demonstrating that the long-axis direction of the 1D C8-BTBT nanowires is aligned with the nanogrooves. Furthermore, the width of the nanowires exceeded the width of the nanogrooves, reaching up to 1 μm (Fig. 1f). The height of the 1D nanowire was 100 nm, as confirmed by the results of the atomic force microscopy studies (Fig. 1g and h). As shown in Fig. 1i, the length of the nanowire could extend up to 0.6 mm, which is beneficial for the subsequent device construction.

The crystallinity of the 1D C8-BTBT nanowires was initially characterized by utilizing the cross-polarized optical microscope (POM), which has been proven to be a highly effective instrument for the identification of materials exhibiting packing anisotropy.[37,38] In order to eliminate any potential influence of the birefringence in the underlying *M*-plane sapphire on the results (Fig. S3†), the single-oriented 1D C8-BTBT nanowires were transferred to a SiO_2/Si substrate *via* the water-soluble polyvinyl alcohol (PVA) film. As shown in Fig. 2a, the 1D nanowires retained the single orientation even after the transfer process. The brightness of the nanowires homogeneously and regularly changed after 45° rotation (Fig. 2b and c),

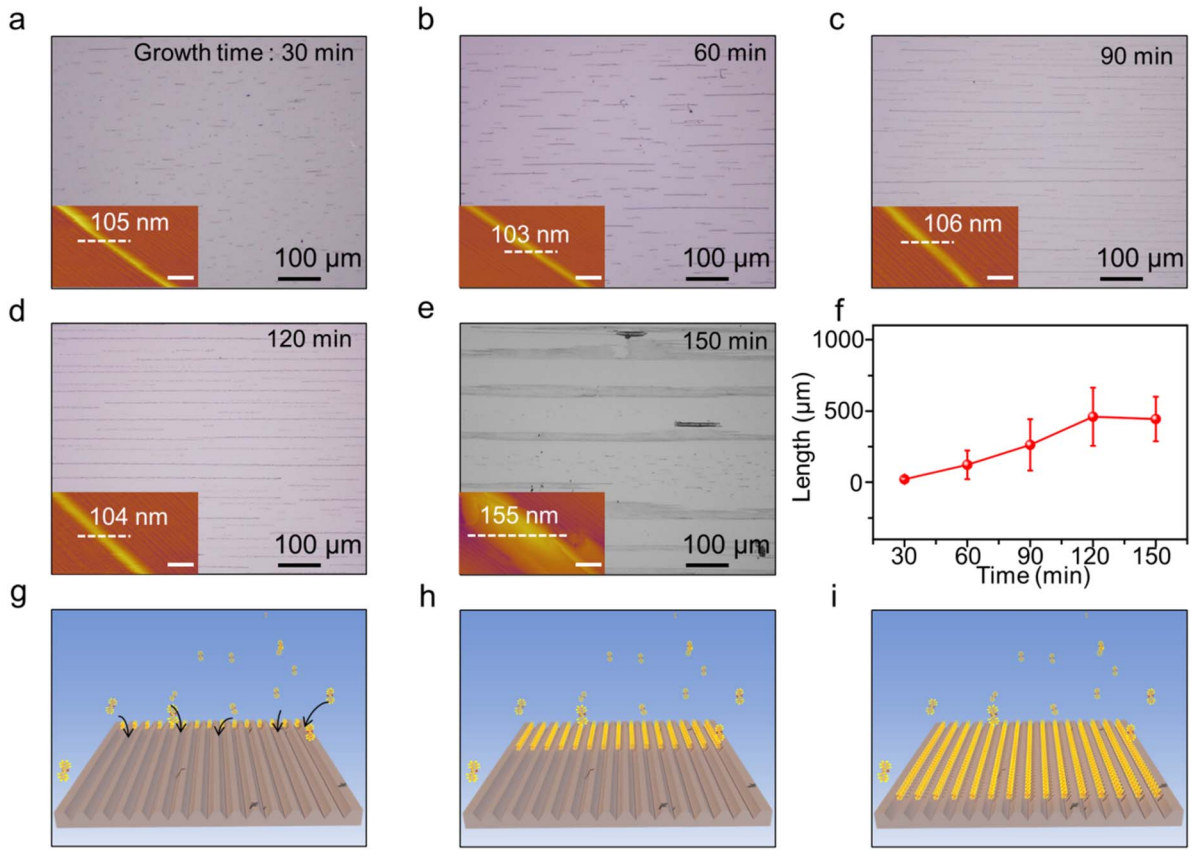

Fig. 3 (a–e) OM images of 1D C8-BTBT nanowires grown for different growth time periods. Insets: corresponding AFM images, scale bar: 1 μm. (f) 1D C8-BTBT nanowire length depends on the growth time. (g–i) Growth mechanism of C8-BTBT molecules aligned and grown as 1D nanowires on the *m*-plane sapphire substrate.

indicating the packing anisotropy in C8-BTBT nanowires. The transmission electron microscopy (TEM) image in Fig. 2d reveals the compact structure of the nanowire. The single-crystalline feature was confirmed by the ordered diffraction spots in the selective-area electron diffraction (SAED) patterns collected from two regions in the 1D C8-BTBT nanowires. Moreover, the crystallographic direction of the 1D C8-BTBT nanowire can be identified as zone axes [020]. Furthermore, the SAED patterns of the different C8-BTBT nanowires were examined on the same Cu grid. Identical diffraction patterns observed for all the nanowires (Fig. 2e–g) indicated that they are single crystals with uniform orientations. The in-plane crystallographic structure of 1D C8-BTBT nanowires was studied through high-resolution atomic force microscopy (HR-AFM). The HR-AFM image in Fig. 2h reveals that 1D C8-BTBT nanowire has the cell parameters of $a = 0.61$ nm and $b = 0.78$ nm, which are consistent with the previously reported herringbone structure of C8-BTBT crystals.[14]

Notably, despite the fact that several aligned inorganic nanowires have been grown directly on the sapphire surface *via* a lattice-matched graphoepitaxy mechanism, the crystallographic growth orientations of the nanowires were often inconsistent.[36] To ascertain the molecular orientation information pertaining to the C8-BTBT nanowires, the detailed examination of their polarized UV-vis absorption properties was conducted. As shown in Fig. 2i, the higher intensity of the 0–0 vibrational peak in comparison to the 0–1 peak suggests the formation of J-type aggregates, indicating robust intermolecular interactions within the C8-BTBT nanowires.[39] With the gradual variation in the polarization angle from 0° to 90°, an evident blue shift was observed in the 0–0 vibration peak, which could be attributed to the Davydov splitting along the *a* and *b* axes.[35] Furthermore, there were notable periodic changes in the intensity of the absorption peak with strong anisotropy, giving rise to a dichroic ratio of about 2.98 (Fig. 2j). Therefore, it can be concluded that all C8-BTBT nanowires have the same crystal structure and consistent crystallographic orientation on the sapphire.

To verify the orientation alignment mechanism of the 1D nanowires grown on *m*-plane sapphires, the surface morphology evolution of the nanowires was investigated as a function of the growth time, and the corresponding orientation distribution of the as-grown nanowires was tracked. Fig. 3a–e shows the OM and AFM images of the as-grown crystals at the growth time ranging from 30 min to 150 min, respectively. Clearly, the morphologies of the nanowires underwent a significant transformation over time. For example, after 30 min growth, the small-sized organic crystals emerged in the V-shaped nanogrooves. As the growth time increased, the length of the nanowires increased in a linear fashion, reaching an average length of 460 μm after 120 min (Fig. 3f and S4†). Upon further prolongation of the growth time, the average

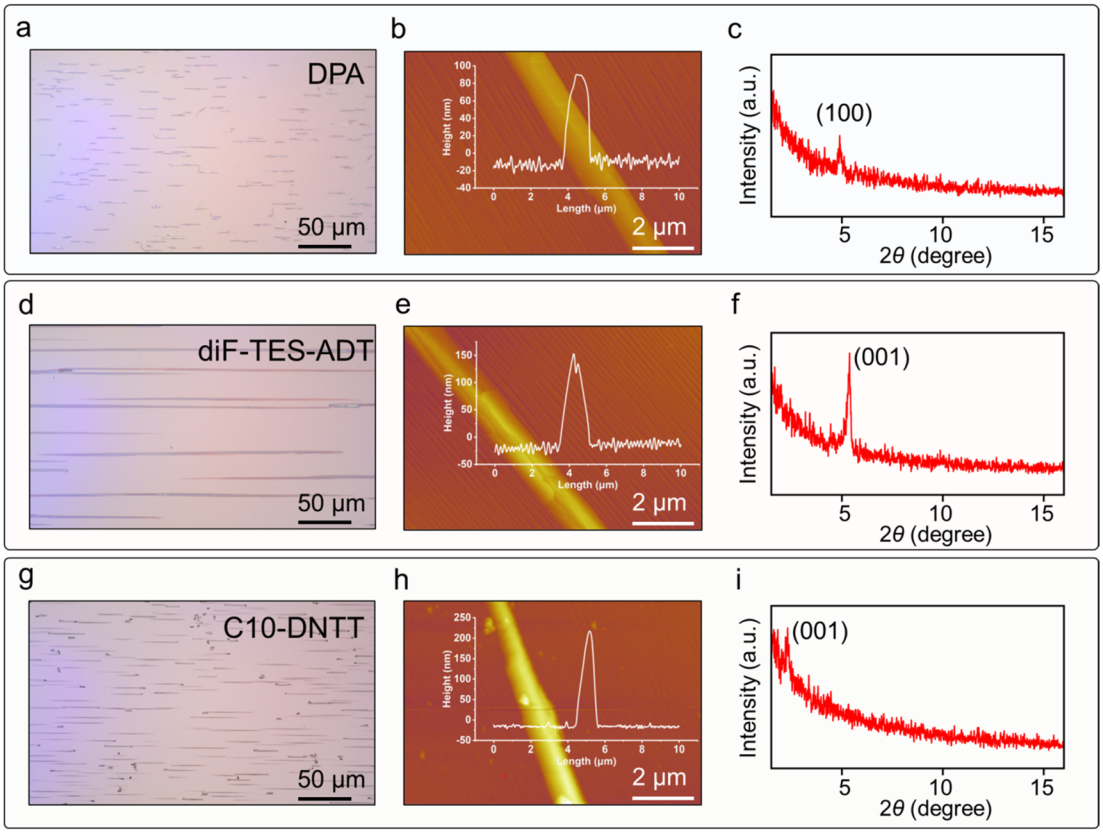

Fig. 4 (a, d and g) OM images of DPA, diF-TES-ADT, and C10-DNTT nanowire arrays with consistent orientation on the *m*-plane sapphire substrate. (b, e and h) AFM images of DPA, diF-TES-ADT, and C10-DNTT nanowires with smooth surfaces on the *m*-plane sapphire substrate. (c, f and i) GIXRD images of DPA, diF-TES-ADT, and C10-DNTT on the *m*-plane sapphire substrate.

length of the nanowires remained unaltered, while the width of the nanowires increased markedly to 5 μm, which could be attributed to the merging of adjacent nanowires. Moreover, the effect of growth temperature and gas flux on the orientation alignment of the nanowires on the sapphire was investigated. It was observed that the length of the nanowires increased rapidly with the slight increase in the growth temperature and gas flux (Fig. S5 and S6†). Nevertheless, no discernible impact was noted on the orientation of the nanowires. The aforementioned results illustrate that the nanoscale grooves on the sapphire play a crucial role in the single-oriented growth of 1D nanowires. Thus, the formation of these directional 1D nanowires can be understood from the following aspects: the vapor precursors initially deposit and are embedded into the V-shaped nanogrooves of the sapphire substrate (see Fig. 3g), thereby forming the anchored seed crystals. Subsequently, the V-shaped nanogrooves facilitate the directionally epitaxial growth of these seed crystals, leading to the generation of C8-BTBT nanowires with a single orientation of [020] (Fig. 3g and i).

In light of the aforementioned characterizations and discussions, we present evidence that the orientation of the nanowires could be well controlled by the nanoscale grooves on the sapphire substrate, indicating that this method has a high potential to facilitate the single-oriented growth of other organic semiconductor materials. In a growth behavior similar to that observed for the C8-BTBT nanowires, the single-oriented growth of the other three molecules (DPA, diF-TES-ADT, and C10-DNTT molecules) into 1D crystalline nanowires were achieved on the sapphire substrate (Fig. 4a, d and g). All the aforementioned nanowires were aligned along the nanogrooves, with a height exceeding 100 nm and smooth surfaces (Fig. 4b, e and h). Furthermore, the XRD results confirm that these nanowires exhibit ordered crystal structures. These results indicate that these molecules could be assembled into organic nanowires without lattice matching between the substrate.

In order to examine the carrier transport properties of the as-fabricated samples, the C8-BTBT nanowires were transferred from the sapphire substrate to the PVP dielectric substrate for the construction of the top-contact bottom-gate flexible OFETs (Fig. 5a). 5 nm F4-TCNQ was deposited between the C8-BTBT nanowires and Ag electrodes. As depicted in Fig. S10,† the HOMO level of the C8-BTBT nanowires (−5.7 eV) was lower than the LUMO level of F4-TCNQ (−5.2 eV).[40] This energy difference

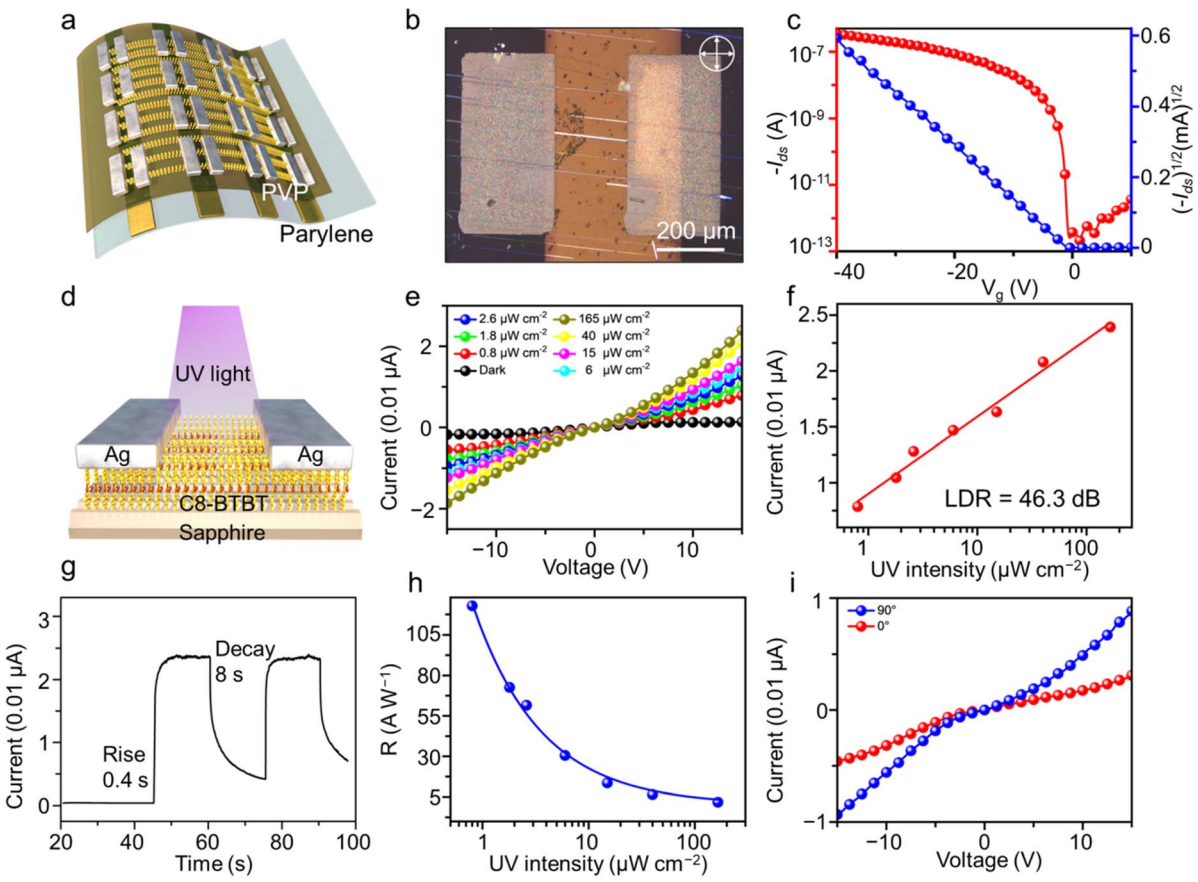

Fig. 5 (a) Schematic of the top-contact bottom-gate flexible OFETs. (b) OM image of the top-contact bottom-gate flexible OFETs based on 1D C8-BTBT nanowires. (c) Transfer characteristic of a typical 1D C8-BTBT nanowire-based OFET. (d) Schematic of the phototransistor based on 1D C8-BTBT nanowires. (e) Current–voltage characteristics of the 1D C8-BTBT nanowire-based photodetector with different UV illumination intensities. (f) Linear dynamic range (LDR) of the C8-BTBT nanowire-based photodetector. (g) Response time of the C8-BTBT nanowire-based photodetector. (h) Responsivity (R) of the C8-BTBT nanowire-based photodetector. (i) Current–voltage characteristics of the 1D C8-BTBT nanowire-based photodetector with different polarization angles.

drives the electrons from the C8-BTBT crystal to F4-TCNQ, leading to the efficient generation of holes in C8-BTBT. In addition, the dopant F4-TCNQ can effectively fill the surface trap states, thereby enhancing charge injection and reducing contact resistance. The channel length and width of the OFETs were 250 and 5 μm, respectively. The transfer curves of the C8-BTBT OFET exhibited the standard p-channel characteristics associated with effective modulation under gate voltage (Fig. 5c). The extracted mobility in the saturation regime was about 1.5 $cm^2\ V^{-1}\ s^{-1}$, accompanied by an on-to-off current ratio of 10^6 and V_{th} of −0.37 V. The distinct saturation behavior of the output curves in Fig. S11† further verifies the excellent device performance of the OFETs. Although the mobility is lower than those reported previously,[35,41,42] a substantial enhancement in mobility can be realized through the optimization of the nanowire thickness, achieved by further refining the growth techniques and the substrates. Furthermore, high mobility and uniform orientation of the 1D C8-BTBT nanowires enable their integration into polarization-sensitive photodetector arrays on the sapphire (Fig. 5d). A commercial 365 nm UV light source was employed for the induction of a photocurrent. Fig. 5e depicts a series of current–voltage (*I*–*V*) curves obtained under 365 nm UV light illumination at varying intensities. The photocurrent demonstrates a linear relationship with the applied voltage for each intensity. Moreover, the slope of the curves exhibits a marked rise with increasing light intensity, indicating a notable light intensity-sensitive response. For instance, as illustrated in Fig. 5f, the photocurrent of the device exhibits a linear increase with light intensity when a bias voltage of 15 V is applied. The calculated linear dynamic range (LDR) is 46.3 dB. Fig. 5g shows that the calculated responsivity (*R*) declines in conjunction with the intensification of light intensity, and the maximum *R* is 122.8 $A\ W^{-1}$. The response speed is another parameter that can be used to evaluate the performance of a photodetector. As shown in Fig. 5h, the calculated rise and decay times are 0.4 s and 8 s, respectively. In addition, the excellent optical anisotropy of the nanowires allows for the evaluation of the photodetector's performance for polarization detection by monitoring the variation in photocurrent with varying polarization angles. Herein, the dichroic ratio (DR) of photocurrent was used to evaluate the performance of the polarized photodetectors. It was found that the DR value of the photodetector based on 1D C8-BTBT nanowires was 2.83, which was higher than those of some investigated 1D nanowires[43–46] and two-dimensional materials.[47–51] These results indicate that the anchored epitaxial growth strategy is an effective approach for the fabrication of high-performance (opto)electronic devices.

Conclusions

In summary, we developed the anchored epitaxial growth strategy to facilitate the single-oriented growth of 1D organic nanowires using the parallel nanogrooves on the annealed sapphire substrate as anchoring seed crystal templates. Due to the depth of the nanogrooves exceeding the length of the molecules, the molecules could be embedded into the V-shaped nanogrooves to form the anchored nuclei during the physical vapor deposition process. Subsequently, these nuclei exhibited directional epitaxial growth along the nanogrooves, resulting in the formation of the single-oriented 1D organic nanowires. Various organic small molecules 1D nanowires with uniform molecular packing and orientation, namely, C8-BTBT, DPA, diF-TES-ADT, and C10-DNTT nanowires, were obtained and were beneficial for the subsequent diverse device integration. Using C8-BTBT as a model material, the flexible organic field-effect transistor based on single C8-BTBT nanowires exhibited a mobility of up to 1.5 $cm^2\ V^{-1}\ s^{-1}$. Benefiting from high mobility and uniform orientation, the integrated polarization-sensitive photodetector arrays based on 1D C8-BTBT nanowires exhibited a high dichroic ratio of up to 2.83, which was higher than those of some investigated 1D nanowires and two-dimensional materials. This work paves the way for the monolithic fabrication of nanowire-based devices through the development of a novel approach for fabricating single-oriented 1D organic nanowires.

Data availability

The data supporting this article have been included as part of the ESI.†

Conflicts of interest

The authors declare that they have no known competing financial interests or personal relationships that could have appeared to influence the work reported in this paper.

Acknowledgements

This work was supported by the National Natural Science Foundation of China (Grant No. 52225303, U24A2082, 51821002, 22461142144, 52403241, 52173178, and 52473189), the Natural Science Foundation of Jiangsu Province of China (BK20240825), the Science and Technology Development Fund (FDCT) of the Macao Special Administrative Region (0145/2022/A3), the Jiangsu Provincial Department of Science and Technology Leading Technology Basic Research Major Project (Grant No. BK20232041), the Suzhou Gusu Innovation and Entrepreneurship Leading Talent Project (Grant No. ZXL2023342), the Suzhou Key Laboratory of Functional Nano & Soft Materials, the Collaborative Innovation Center of Suzhou Nano Science & Technology, the Jiangsu Association for Science and Technology, the Outstanding Science & Technology Innovation Team for Jiangsu Universities, and the 111 Project.

Notes and references

1 Y. Wu, J. Feng, X. Jiang, Z. Zhang, X. Wang, B. Su and L. Jiang, *Nat. Commun.*, 2015, **6**, 6737.
2 Y. L. Shi, Q. Lv, Y. C. Tao, Y. X. Ma and X. D. Wang, *Angew. Chem., Int. Ed.*, 2022, **61**, 202208768.
3 J. Feng, W. Wen, X. Wei, X. Jiang, M. Cao, X. Wang, X. Zhang, L. Jiang and Y. Wu, *Adv. Mater.*, 2019, **31**, 1807880.

4 Y. Yao, L. Zhang, T. Leydecker and P. Samorì, *J. Am. Chem. Soc.*, 2018, **140**, 6984.
5 W. Deng, X. J. Zhang, L. Wang, J. C. Wang, Q. X. Shang, X. H. Zhang, L. M. Huang and J. S. Jie, *Adv. Mater.*, 2015, **27**, 7305.
6 S. Y. Min, T. S. Kim, Y. Lee, H. Cho, W. Xu and T. W. Lee, *Small*, 2014, **11**, 45.
7 H. Li, B. C. K. Tee, G. Giri, J. W. Chung, S. Y. Lee and Z. Bao, *Adv. Mater.*, 2012, **24**, 2588.
8 S. Gao, S. Hong, S. Park, H. Y. Jung, W. Liang, Y. Lee, C. W. Ahn, J. Y. Byun, J. Seo, M. G. Hahm, H. Kim, K. Kim, Y. Yi, H. Wang, M. Upmanyu, S.-G. Lee, Y. Homma, H. Terrones and Y. J. Jung, *Nat. Commun.*, 2022, **13**, 3467.
9 L. Wu, Z. Hu, L. Liang, R. Hu, J. Wang and L. Yu, *Nat. Commun.*, 2025, **16**, 965.
10 D. Zopes, R. von Hagen, R. Müller, R. Fiz and S. Mathur, *Nanoscale*, 2010, **2**, 2091.
11 P. Cannon, E. McGlynn, B. Freeland and J. Gaughran, *New J. Chem.*, 2023, **47**, 3734.
12 U. Hujuri, A. K. Ghoshal and S. Gumma, *J. Appl. Polym. Sci.*, 2013, **130**, 3993.
13 S. Liu, W. M. Wang, A. L. Briseno, S. C. B. Mannsfeld and Z. Bao, *Adv. Mater.*, 2009, **21**, 1217.
14 J. Pan, Y. M. Wu, X. J. Zhang, J. H. Chen, J. W. Wang, S. L. Cheng, X. F. Wu, X. H. Zhang and J. S. Jie, *Nat. Commun.*, 2022, **13**, 6629.
15 W. Xin, W. Zhong, Y. Shi, Y. Shi, J. Jing, T. Xu, J. Guo, W. Liu, Y. Li, Z. Liang, X. Xin, J. Cheng, W. Hu, H. Xu and Y. Liu, *Adv. Mater.*, 2023, **36**, 2306772.
16 Y. Kim, C. Zhu, W. Y. Lee, A. Smith, H. Ma, X. Li, D. Son, N. Matsuhisa, J. Kim, W. G. Bae, S. H. Cho, M. G. Kim, T. Kurosawa, T. Katsumata, J. W. F. To, J. Y. Oh, S. Paik, S. J. Kim, L. Jin, F. Yan, J. B. Tok and Z. Bao, *Adv. Mater.*, 2023, **35**, 2203541.
17 C. Wang, X. Zhang and W. Hu, *Chem. Soc. Rev.*, 2020, **49**, 653.
18 P. Yu, Y. Zhen, H. Dong and W. Hu, *Chem*, 2019, **5**, 2814.
19 L. Zhang, N. Pasthukova, Y. Yao, X. Zhong, E. Pavlica, G. Bratina, E. Orgiu and P. Samori, *Adv. Mater.*, 2018, **30**, 1801181.
20 X. Y. Xia, L. Y. Ding, Q. Lv, X. D. Wang and L. S. Liao, *Adv. Electron. Mater.*, 2022, **8**, 2200753.
21 H. Dong, C. Zhang, F. J. Shu, C. L. Zou, Y. Yan, J. Yao and Y. S. Zhao, *Adv. Mater.*, 2021, **33**, 2100484.
22 L. Y. Xu, Z. L. Wang, Q. Song, X. H. Sun, H. Y. Liu, R. C. Fang and X. Y. Jiang, *Adv. Funct. Mater.*, 2024, **34**, 2315162.
23 O. Yildiz, Z. Y. Wang, M. Brzezinski, S. L. Wang, Z. P. Li, J. J. Michels, P. W. M. Blom, W. Pisula and T. Marszalek, *Adv. Funct. Mater.*, 2024, **34**, 2314131.
24 F. Sheng, W. Deng, X. Ren, X. Liu, X. Meng, J. Shi, S. Grigorian, J. Jie and X. Zhang, *Adv. Mater.*, 2024, **36**, 2401822.
25 W. Zhao, J. Jie, Q. Wei, Z. Lu, R. Jia, W. Deng, X. Zhang and X. Zhang, *Adv. Funct. Mater.*, 2019, **29**, 1902494.
26 X. J. Zhang, W. Deng, R. F. Jia, X. H. Zhang and J. S. Jie, *Small*, 2019, **15**, 201900332.
27 K. Kim, J. Hong, S. G. Hahm, Y. Rho, T. K. An, S. H. Kim and C. E. Park, *ACS Appl. Mater. Interfaces*, 2019, **11**, 13481.
28 K. S. Park, J. Baek, Y. Park, L. Lee, Y. E. Lee, Y. Kang and M. M. Sung, *Adv. Mater.*, 2016, **28**, 2874.
29 X. L. Zhang, W. Deng, B. Lu, X. C. Fang, X. J. Zhang and J. S. Jie, *Nanoscale Horiz.*, 2020, **5**, 1096.
30 S. B. Lee, S. Lee, D. G. Kim, S. H. Kim, B. Kang and K. Cho, *Adv. Funct. Mater.*, 2021, **31**, 2100196.
31 Y. Zhao, Q. Sheng, S. Ke, R. Wu, L. He, X. Ren, B. Peng and H. Li, *Small*, 2024, 2404770, DOI: **10.1002/smll.202404770**.
32 X. Zhang, J. Jie, W. Deng, Q. Shang, J. Wang, H. Wang, X. Chen and X. Zhang, *Adv. Mater.*, 2016, **28**, 2475.
33 K. Y. Wu, T. Y. Wu, S. T. Chang, C. S. Hsu and C. L. Wang, *Adv. Mater.*, 2015, **27**, 4371.
34 J. Wang, W. Deng, W. Wang, R. Jia, X. Xu, Y. Xiao, X. Zhang, J. Jie and X. Zhang, *Nano Res.*, 2019, **12**, 2796.
35 J. W. Wang, Z. Ren, J. Pan, X. F. Wu, J. S. Jie, X. H. Zhang and X. J. Zhang, *Adv. Mater.*, 2023, **35**, 2301017.
36 X. Wei, S. Wang, N. Zhang, Y. Li, Y. Tang, H. Jing, J. Lu, Z. Xu and H. Xu, *Adv. Funct. Mater.*, 2023, **33**, 2300141.
37 W. Deng, Y. Xiao, B. Lu, L. Zhang, Y. Xia, C. Zhu, X. Zhang, J. Guo, X. Zhang and J. Jie, *Adv. Mater.*, 2020, **33**, 11.
38 Y. L. Xiao, W. Deng, J. J. Hong, X. B. Ren, X. J. Zhang, J. L. Shi, F. M. Sheng, X. H. Zhang and J. S. Jie, *Adv. Funct. Mater.*, 2023, **33**, 2213788.
39 J. W. Wang, X. F. Wu, J. Pan, T. L. Feng, D. Wu, X. J. Zhang, B. Yang, X. H. Zhang and J. S. Jie, *Adv. Mater.*, 2020, **32**, 2003315.
40 K. Pei, A. H. Y. Lau and P. K. L. Chan, *Phys. Chem. Chem. Phys.*, 2020, **22**, 7100.
41 B. Fu, F. Yang, L. Sun, Q. Zhao, D. Ji, Y. Sun, X. Zhang and W. Hu, *Adv. Mater.*, 2022, **34**, 2203330.
42 D. He, J. Qiao, L. Zhang, J. Wang, T. Lan, J. Qian, Y. Li, Y. Shi, Y. Chai, W. Lan, L. K. Ono, Y. Qi, J.-B. Xu, W. Ji and X. Wang, *Sci. Adv.*, 2017, **3**, e1701186.
43 S. N. Chen, X. Y. Ma, Z. R. Cai, H. R. Long, X. Y. Wang, Z. Li, Z. Y. Qu, F. J. Zhang, Y. L. Qiao and Y. L. Song, *Adv. Mater.*, 2022, **34**, 8.
44 T. Wang, K. Zhao, P. Wang, W. Shen, H. Gao, Z. Qin, Y. Wang, C. Li, H. Deng, C. Hu, L. Jiang, H. Dong, Z. Wei, L. Li and W. Hu, *Adv. Mater.*, 2022, **34**, 2105665.
45 L. Gao, K. Zeng, J. Guo, C. Ge, J. Du, Y. Zhao, C. Chen, H. Deng, Y. He, H. Song, G. Niu and J. Tang, *Nano Lett.*, 2016, **16**, 7446.
46 J. Wang, Y. Zhang, J. Chen, Y. Wei, D. Yu, L. Liang, Y. Liu, Y. Wu, W. Shen, X. Li and H. Zeng, *ACS Appl. Mater. Interfaces*, 2021, **13**, 36147.
47 L. Li, P. Gong, D. Sheng, S. Wang, W. Wang, X. Zhu, X. Shi, F. Wang, W. Han, S. Yang, K. Liu, H. Li and T. Zhai, *Adv. Mater.*, 2018, **30**, 1804541.
48 Y. Yan, W. Xiong, S. Li, K. Zhao, X. Wang, J. Su, X. Song, X. Li, S. Zhang, H. Yang, X. Liu, L. Jiang, T. Zhai, C. Xia, J. Li and Z. Wei, *Adv. Opt. Mater.*, 2019, **7**, 1900622.
49 Y. Yan, J. Yang, J. Du, X. Zhang, Y. Y. Liu, C. Xia and Z. Wei, *Adv. Mater.*, 2021, **33**, 2008761.
50 Z. Zhou, M. Long, L. Pan, X. Wang, M. Zhong, M. Blei, J. Wang, J. Fang, S. Tongay, W. Hu, J. Li and Z. Wei, *ACS Nano*, 2018, **12**, 12416.
51 D. Kim, K. Park, J. H. Lee, I. S. Kwon, I. H. Kwak and J. Park, *Small*, 2021, **17**, 2006310.